Acta of Bioengineering and Biomechanics
Vol. 18, No. 3, 2016

Original paper
DOI: 10.5277/ABB-00462-2015-03

The upper ankle joint: Curvature morphology of the articulating surfaces and physiological function

HANS NÄGERL[1], CLAUDIA HANSEN[1], DIETMAR KUBEIN-MEESENBURG[1], JOCHEN FANGHÄNEL[2], HENNING DATHE[1], CLEMENS DUMONT[3], MARTIN MICHAEL WACHOWSKI[4]*

[1] Department of Orthodontics, University of Göttingen, Germany.
[2] Department of Orthodontics, University of Regensburg, Germany.
[3] Clinical Center Kassel, Germany.
[4] Department of Trauma Surgery, Orthopaedics and Plastic Surgery, University of Göttingen, Germany.

Purpose: The curvature morphology of the articulating surfaces determines the physiological movement pattern. We quantitatively examined the curvature morphology of the tibiotalar articulating surfaces and specified their geometric contact patterns. *Methods*: Geometrically equivalent cartographic nets were marked on the talar and tibial articulating surfaces of true-to-scale moldings of 20 human ankle joints (intervals of 5 mm) to relate corresponding articulating units of the surfaces. The corresponding contours of the net lines were compared, and the incongruity of articulating surfaces could thus be quantified locally. *Results*: All tibial sagittal net lines represented circular arcs. Along the sagittal talar net lines, the curvature radii increased medially from anterior to posterior but decreased laterally. Each net line could be approximated by three circular arcs. Examining these three parts of the talar net lines, the anterior sagittal curvature radii increased from medial to lateral, whereas the posterior radii decreased. The tibial and talar transversal net lines were congruent. The articulation surfaces showed a transversal contact line in every dorsal/plantar joint position. The degree of local congruity was solely ascertained by the incongruity of the corresponding sagittal net lines. The maximal degrees of congruity were found laterally for dorsal flexion, laterally/centrally for neutral joint position, and centrally/medially for plantar flexion. *Conclusions*: By the transversal line contact, the contact area is broadened over the articulating surfaces from lateral to medial. In dorsal flexion, compressive loads are mainly transferred by lateral/anterior zones and in plantar flexion by medial/posterior zones of the articulating surfaces. Reconstruction of the transversal contact line is essential.

Key words: *biomechanics, joint kinematics, human, curvature morphology, upper ankle joint, incongruity*

1. Introduction

The observed prevalence of 1% for primary arthrosis in the upper ankle joint (UAJ) is remarkably lower than that of approximately 6% in the knee joint [14], [16]. The most common upper ankle arthrosis is secondary and has a post-traumatic origin in approximately 70–80% of patients [7], [27], indicating the joint's high resistance under physiological loads. Is there biomechanical evidence for this observation?

In a compressively loaded UAJ, a mutual contact area appears between the articulating surfaces of the tibia and talus [12], [23]. This area is loaded by multiple body weights during walking, running, and jumping [25]. Although some studies have considered this contact area [11], [30], and despite the existence of multiple radiological studies [22], [29], the geometric pattern of the contact area is unknown. To describe contact areas geometrically, the curvatures of both contacting surfaces must be compared locally. The published data concerning the articular curvature morphology vary considerably. The contours of sagittal cuts through the tibial surface have been closely approximated by circular arcs [1], [4], [11] with curvature radii between 20 and 26.6 mm [4], [6], [14], [23]. The sagittal talar contours, however, were not simple circular arcs. In dorsal direction, the local cur-

* Corresponding author: Martin Michael Wachowski, Department of Trauma Surgery, Orthopaedics and Plastic Surgery, University of Göttingen, Robert-Koch-Str. 40, 37075 Göttingen, Germany. Tel: +49551396114, e-mail: martin.wachowski@web.de

Received: September 6th, 2015
Accepted for publication: October 19th, 2015

vature radius increased medially and decreased laterally [1]. The local sagittal talar curvature radii were between 19–22 mm [14]. The tibial and talar sagittal curvatures were incongruous.

A contact line is transversally possible, as Windish et al. [30] demonstrated in 20 ankle joints [28]. Using a three-dimensional (3D) laser scanner, the datasets of both articulating surfaces were recorded separately. Between the virtually contacting articulating surfaces, domains of minimal distances were observed, reaching from the medial to the lateral side. Kura et al. [11] and Kimizuka et al. [9] found contact areas [4], [9] extending over the complete talus.

The contact area [13], [30] moves to the anterior during dorsiflexion and to the posterior during plantar flexion on both articulating surfaces [6], [19]. This concordant movement of the contact biomechanically conditions that the two articulating surfaces partially roll on each other [18]. How the shape of the contact area changes during movement is still unknown.

In this study, we present cartographic information regarding the curvature morphology of both articulating surfaces (a) to evaluate for preset positions of the contact area the local grade of congruity in sagittal and transversal direction for dorsal or plantar flexion and (b) to qualitatively discuss the geometric distribution of the joint stress onto the articulating surfaces.

Central questions of the study:

1. How do the shape of the sagittal tibial contours and that of the sagittal talar contours depend on the medial/lateral and anterior/posterior contact position?
2. How does the sagittal grade of congruity between the talus and tibia depend on the possible contact area positions?
3. How does the transversal grade of congruity change on the articulating surfaces?
4. How does the shape of the contact area alter during dorsal and plantar flexion?

2. Materials and methods

Materials

A total of 20 human ankle specimens (10 right, 10 left from 13 from female and seven male donors; mean age = 85.4 yrs.) were obtained from the Anatomical Institute Greifswald. The specimens were preserved in a solution that maintained the hardness of the bone and the elasticity of the cartilage. The sufficient hardness of the bone prevented changes in the molded articulating surfaces caused by the casting procedures. The anatomical specimens showed no macroscopic indications of osteoarthritis or any form of posttraumatic alteration. They were dissected up to the joint capsule.

Marks on the articulating surfaces

Leaving the joint capsule intact, two check marks, separated by 2 cm, were made by diathermia at the ventral tibial articulating surface and at the corresponding places of the talus in a neutral joint position. Additionally, in four different joint positions from plantar flexion to dorsiflexion, marks corresponding to the two tibial marks were made on the talus. Thus, physiological joint positions could be readjusted after the articulating surfaces had been separated for casting procedures.

Production of the plaster models

Plaster models were produced from the separated talar and tibial articulating surfaces using silicon molds (Double mixture: Silaplast®, Detax and Xantopren®, Bayer Dental) with high reproductive precision [3]. These hollow molds were grouted by super-hard plaster (New Fujirock®, GC International), generating the true-to-scale plaster models [6].

A net with quasi-quadratic meshes was plotted on the "plaster surfaces". This net provided the template articulating with which the local curvatures of both articulating surfaces could be geometrically allocated.

Sagittal net lines

On each talus model, a sagittal line was first drawn parallel to the talus medial edge. Parallel to this basic line, four lines were drawn at intervals of 5 mm (Fig. 1a). To transfer these five lines to the corresponding tibia plaster model, both models were allocated in

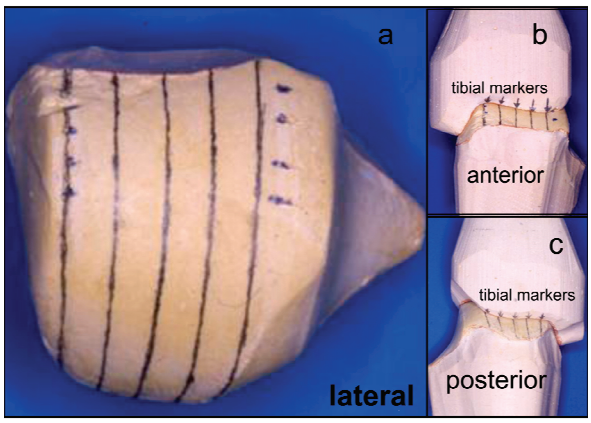

Fig. 1. Marking of sagittal net lines. (a) Plaster model of a talus with medial and lateral check marks. Five sagittal net lines were marked on the articulating surface; (b), (c) establishing of the corresponding five net lines on the tibial articulating surface

the neutral joint position using the marks. The five observable lines on the larger talar surface were marked on the anterior and posterior edges of the tibial surface (Fig. 1b, c) to draw five parallel sagittal lines on the tibial surface.

Transversal net lines

Eight transversal lines were drawn on the talar articulating surface. On each talus model, the penetration points of an estimated rotational axis of dorsal/plantar flexion were tagged medially and laterally, representing the empirically determined, averaged centers of the sagittal slices through the original silicon hollow mold. These two points were connected by a median transverse line, which ran over the articulating surface. Additionally seven lines were drawn at intervals of 5 mm on the surface (Fig. 2a, b). Analogous to the sagittal net lines, five transversal talar net lines were transferred onto the smaller tibial surface. Thus, corresponding geometric grids were placed on the talar and tibial articulating surfaces (Fig. 2c, d).

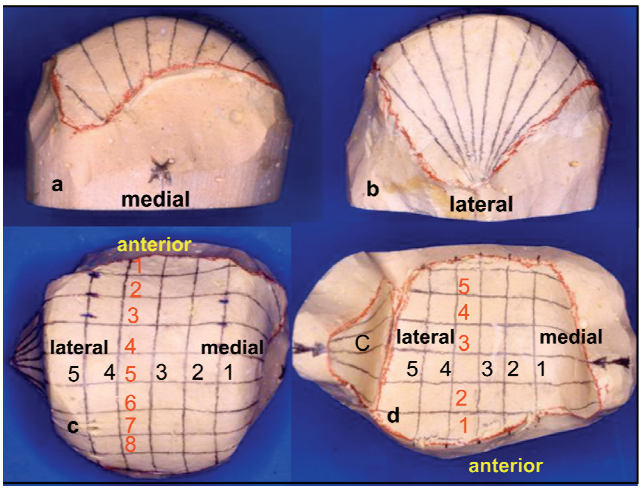

Fig. 2. Marking of transversal net lines.
(a), (b) The eight transversal net lines run through the medial and lateral penetration points of the mean rotational talar axis.
(c) Cartographic net on the talar articulating surface.
(d) Corresponding cartographic net on the tibial articulating surface.
C: Fibular articulating surface

Evaluation of the net contours

The tibial and the talar plaster surfaces were molded multiple times in silicon. Thereby the nets were stained onto these negative forms. These silicon models were sliced along the copied lines. Thus, pistons that reflected true-to-scale net lines were produced. All sagittal tibia lines proved to be circular arcs. The accuracy of the measured curvature radii was 0.5 mm [2]. However, none of the sagittal talar lines complied with one single circular arc. When dividing the talar surfaces into anterior, central, and posterior thirds, the resulting pieces could be approximated by circular arcs.

The transversal tibial and talar net lines were printed in transparent sheets and overlaid for comparison.

3. Results

3.1. Sagittal net lines

Tibia

The sagittal curvature radii (R_{Tib}) tended to decline concededly from medial to lateral, without pronounced significance (Table 1; ANOVA: $p = 0.062 > 0.05$). The non-parametric T-group test showed a significant difference ($p < 0.05$) between net line 2 and the other lines. Both tests combined, made probably that the curvature radius decreased from medial to lateral.

Talus

In the anterior/posterior third, the largest sagittal curvature radii ($R_{Tal,a}$\$R_{Tal,c}$) were found at the lateral/medial side (Table 1). Centrally, no significant differences were observed between the medial and lateral curvature radii. The curvature radii of the medial net lines 1, 2, and 3 increased significantly from anterior to posterior. Net line 4 did not significantly change in radius. Along the most lateral net line 5, the sagittal curvature radius decreased significantly from anterior to posterior.

Comparison of talar and tibial sagittal curvature radii

The tibial curvature radii were greater than or equal to the three corresponding talar radii (Table 2). The observed difference depended on the location on the talar articulating surface. In the anterior and central thirds, the difference was highest medially, and declined significantly from medial to lateral. In the posterior third, however, the differences were highest laterally and were chiefly conditioned by net line 5. For the medial net lines 1, 2, and 3, the difference between the curvature radii decreased significantly from anterior to posterior. However, laterally, for net line 5, the radii difference increased from anterior to posterior.

Table 1. Sagittal curvature radii on the articulating surface along the five sagittal net lines (means with standard deviations (SD)). All tibial net lines are circular. The respective curvature radii (R_{Tib}) are not significantly differentiated. Dividing the talar surface in thirds each net line was approximated by a circle. The curvature radii increased along the net lines 1, 2, 3 from anterior to posterior; but decreased along net line 5

	Curvature radii	Sagittal net line (lateral → medial)					
		5	4	3	2	1	ANOVA
Tibia	R_{Tib}/mm SD/mm	22.1 2.157	22.5 2.767	23.2 3.722	25.1 4.782	24.5 4.834	n.s. $p < 0.066$
Talus anterior third	$R_{Tal,a}$/mm SD/mm	22.5 2.840	20.1 2.486	18.5 1.697	18.1 3.330	18.7 2.498	*** $p < 0.0001$
Talus central third	$R_{Tal,p}$/mm SD/mm	20.5 1.867	20.8 2.154	20.8 2.215	20.9 2.533	20.2 2.515	n.s. $p < 0.875$
Talus posterior third	$R_{Tal,a}$/mm SD/mm	18.4 3.877	21.6 3.292	22.5 3.985	24.6 5.353	23.5 5.539	*** $p < 0.0005$
Talus radius changing	$\Delta R_{Tal,p\text{-}a}$/mm	–4.1 $p < 0.02$	1.5 n.s.	4.0 <0.01	6.5 $p < 0.01$	4.8 $p < 0.02$	

Table 2. Differences between the curvature radii of the talus and the tibia in relation to the position on the talus articulating surface. $\Delta Ra = R_{Tib} - R_{Tal,a}$; $\Delta Rc = R_{Tib,} - R_{Tal,c}$; and $\Delta Rp = R_{Tib} - R_{Tal,p}$

Cartogram: differences of the curvature radii		Sagittal net line (lateral → medial)					
		5	4	3	2	1	ANOVA
Anterior third	ΔRa/mm SD/mm	0.05 2.253	2.53 2.868	4.75 4.204	7.05 4.704	5.85 4.404	*** $p < .0001$
Central third	ΔRc/mm SD/mm	1.70 1.409	1.825 2.067	2.750 2.967	4.250 3.796	4.30 3.643	** $p < .0073$
Posterior third	ΔRp/mm SD/mm	3.68 3.419	1.10 2.998	0.80 2.633	0.55 3.605	0.93 4.222	*** $p < .026$
Significance		$p < .01$	n.s.	$p < .02$	$p < .01$	$p < .02$	

3.2. Transversal net lines

Tibia and fibula

The median transversal tibial contour was convex (Fig. 3a). The contours became concave at the medial side and continued to be concave to the caudal articulating part. The descending contours were longer in the anterior and shorter in the posterior part of the tibial surface. Laterally, after a sharp bend, the fibular articulating contours were convex.

Talus

All eight transversal net lines were concave in the median part but became convex on the medial and lateral sides (Fig. 3b). Medially, the convex contour continued caudally, which became shorter at the posterior zone of the surface. Laterally, the convex contour bent sharply down and switched caudally into a concave contour articulating with the fibula. The bend defined the border between the tibiotalar and fibulotalar joint. Similar to the tibial articulating surface, the talar surface was wider in its anterior part.

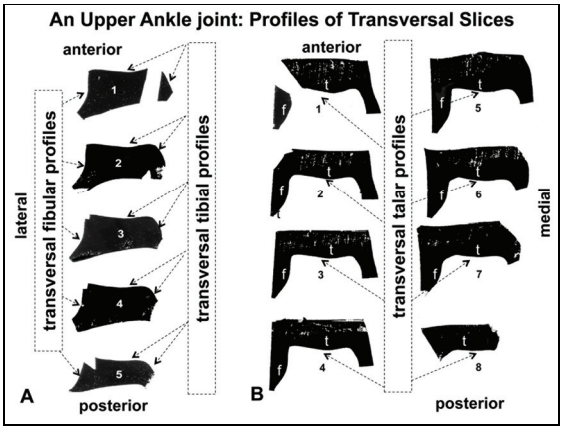

Fig. 3. Transversal contours of sections along the net lines in joint 9L. A: Piston impressions of the five transverse sections through the tibial silicon female mold. Compare the positions of the sections with those in Fig. 2d. B: Piston impressions of the eight transverse sections through the talus female articulating mold. *t* = articulating part with the tibia, *f* = articulating part with the fibula. Compare the positions of the sections with those in Fig. 2c

Talar versus tibial transversal lines

In 19 of the 20 UAJ, the tibial and talar contours could be accurately overlaid, as exemplified in Figs. 4

and 5. Because the contact area migrates anteriorly in dorsiflexion and posteriorly in plantar flexion on both articulating surfaces [6], [19], we related the five tibial transversal lines, 1–5, to the five anterior talus transversal lines, 1–5, for dorsal joint positions and to the five posterior talus transversal lines, 4–8, for plantar joint positions. In each particular case, the transversal talar and tibial net lines *were congruent to a large extent*. Note: in plantar flexion, (a) the tibial-talar net lines did exactly overlap and (b) the talar-fibular lines did also closely contact, at least at a point. However, in dorsiflexion, the related talar-tibial net lines fitted furthermore, but the fibular contours were shifted medially. This was an artifact of the molding process because the syndesmosis was slack when the negative forms were produced. In the dorsiflexion of an intact joint, however, the syndesmosis was tight because of the wider anterior talus zone. Accordingly, the fibular articulating surface was shifted laterally up to approximately 1–2 mm.

In one joint (14R), the transversal tibial and talar contours were always incongruent. The talar joint surface was too wide, even in the posterior area of function. Hence, the distension of the syndesmosis was already necessary in plantar flexion.

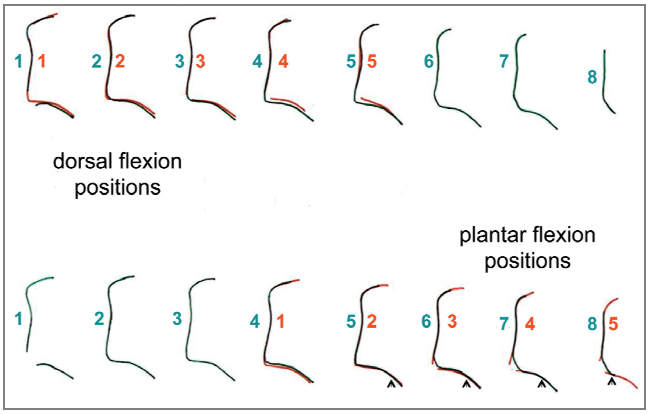

Fig. 4. Overlay of the five transversal net lines of malleolus medialis and lateralis (red) each with five talar transversal net lines (green) of the ankle joint 9L. Dorsal flexion positions: overlay of the five tibial net lines with the five net lines of the anterior part of the talus. Plantar flexion positions: Overlay of the five tibial net lines with the five net lines of the posterior part of the talus

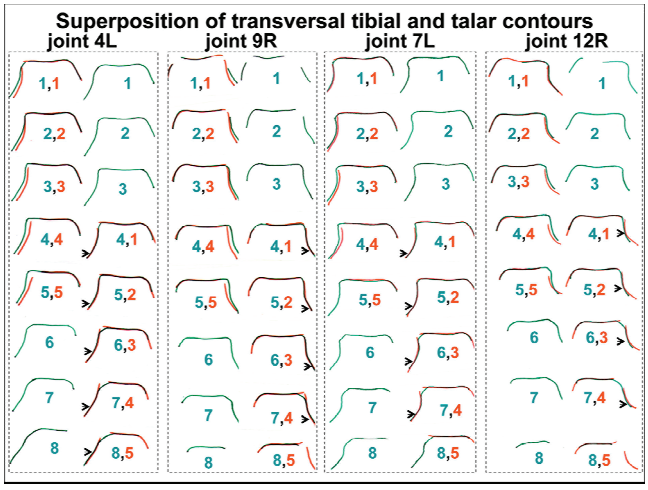

Fig. 5. Overlay of five transversal contours of ankle joints: Transversal contours of the malleolus medialis and lateralis (red line) and transverse contours of the talus (green line) for four additional joints. The left contours in each column represent the status in dorsiflexion, right contours in plantar flexion. As in the previous example, these joints confirmed the congruity of the tibial and talar transversal contours

4. Discussion

Our morphological measurements showed that a medial/lateral contact line exists between the tibial and talar articulating surface and that it moves on both surfaces, depending on the joint's flexional/extensional angle.

Functional impact of transversal net lines

Because the anterior/posterior dimension of the talar articulating surface is larger than that of the tibia (Fig. 1c), eight talar transversal net lines corresponded to five tibial transversal net lines (Fig. 2c, d). Overlays (in Figs. 4, 5) supplied uniform transversal congruent profiles along both articulating surfaces. Because the sagittal net lines were incongruous, a transversal *line contact* must exist in any dorsal/plantar joint position.

Because in increasing dorsiflexion, the contact line moves anteriorly on both surfaces, the experimental overlays (4, 4) and (5, 5) (in Figs. 4, 5) have no physiological relevance because the tibial contours (4) and (5) belong to the posterior positions of the contact line on the tibial surface. Analogously, the allocations (4, 1) and (5, 2) in plantar flexion have no physiological meaning.

The data showed that a contact line could be set in 19 of the 20 joints by compressive forces in every position of dorsal/plantar flexion. In dorsiflexion, the contact line is naturally present because of the taut anterior and posterior syndesmotic ligament structures. This strong force caliper of the malleolus medialis and lateralis considerably reduces axial rotation and transversal translation. Only two degrees of freedom in terms of a sagittal dimeric link chain [2] are practically left for the joint.

Because the transversal force of the malleolus lateralis and medialis is omitted in plantar flexion, the joint can leave the contact line and rotate axially. Hence, the unloaded foot can be used as a palpating tool. Alternately, under load by standing on tip-toe, the joint can slightly axially rotate.

Theoretically, the articulating surfaces can be distracted medially or laterally along the contact line. However, the compressive force closure stabilizes the joint's position because every medial/lateral distraction would produce a dehiscence of the tibia and talus, which works against the compressive force.

Eversion and inversion are physiologically almost impossible in the UAJ because they would produce a concomitant dehiscence of the talus and tibia acting against the compressive joint loads.

Functional impact of sagittal net lines

Because the transversal net lines are congruent, the sagittal incongruity of the articulating surfaces is physiologically necessary, as it enables the circulation of the synovia to ensure lubrication and nutrition of the cartilage [2], [7].

Because the tibial net lines were circular and the corresponding talar net lines were non-circular (Table 1), the local sagittal curvature incongruity was primarily determined by the shape of the talar surface (Table 2). In the medial-lateral direction, the tibial sagittal curvature radii remained hardly changed, but the talar radii increased in the anterior zone and decreased in the posterior zone (Table 1). The functional impact of the local dimensions of sagittal incongruity depended on the instantaneous location of the contact line.

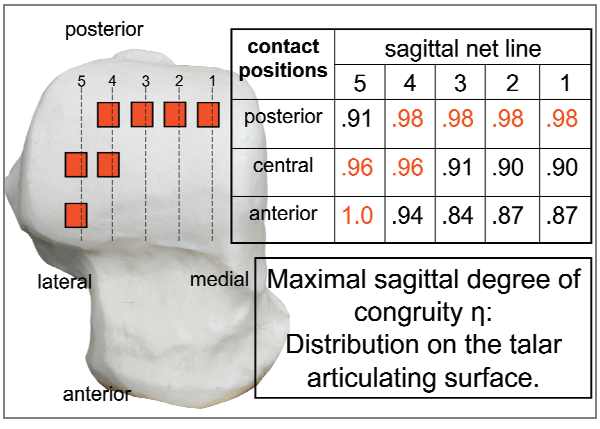

contact positions	sagittal net line 5	4	3	2	1
posterior	.91	.98	.98	.98	.98
central	.96	.96	.91	.90	.90
anterior	1.0	.94	.84	.87	.87

Fig. 6. The lateral/medial location of the maximal sagittal degree of congruity η between both articulating surfaces depends on the anterior/posterior position of the contacting line between talus and tibia

Based on the theory of contact of solid bodies [23], we defined the degree of sagittal congruity η as $\eta = \frac{2 \cdot R_{Tal}}{R_{Tib} + R_{Tal}}$, calculated η (using Table 1), and performed a standardized survey of the degree of local sagittal congruity (Fig. 6). Because the mutual contact lines were present transversally, η was used to estimate the degree of congruity of the local mean curvatures of articulating surfaces. Figure 6 visualizes the distribution of the zones with high degrees of congruity over the talar articular surface.

Dorsiflexion

The contact line is anteriorly located on the talus, where the articulating surfaces are in almost perfect congruity ($\eta = 1$) on the outermost lateral side.

Neutral joint position

The degree of congruity, η, is still high on the lateral side, where the difference in radii is $\Delta R < 0.077 \cdot R_{Tib}$. Kimizuka et al. [9] previously described the highest compressive strain at this location under a compressive load of 1000 N [9].

In *plantar flexion*, joint contact is posteriorly located on the talus, and a high congruity ($\Delta R < 0.04 \cdot R_{Tib}$) exists medially and centrally on the talar surface, as previously observed by Paar et al. [19].

Geometric features of the contact area under compressive load

A compressive load extends the contact line to a contact area. Both articulating surfaces are impressed according to the so-called Hertz compression of surfaces [12]. Compared with a contact point, a contact line, l_c, has the advantage of spreading a given load over a wider area, thereby reducing the pressure on the cartilage surfaces.

In a concave-convex articulation, the width $A(l_c)$ of the contact area locally increases along contact line, l_c, under a compressive load if

(a) the convex sagittal curvature radii (Table 1) or/and
(b) the degree of sagittal congruity (Table 2, Fig. 6) are increasing.

Dorsiflexion

The contact line is located in the anterior third of the talar surface (Fig. 6). Coming from the medial side, the talar sagittal radii (R_{Tal}) and congruity, η, have small constant values. Additionally, the width $A(l_c)$ is small and constant up to midway. Laterally, R_{Tal} and η increase considerably. As such, the articulating surfaces become locally congruent ($\eta \approx 1$), and the contact area expands. Consequently, the main

focus of the contact area and the transmission of joint force are on the lateral side.

Neutral joint position

The contact line is centered. Width A(l_c) is medially grown because the sagittal talar curvature radius (Table 1) and the degree of congruity (Table 2, Fig. 6) are increased. Though the degree of congruity remains laterally larger, altogether, the main foci of the contact area and force transmission are medially shifted compared with dorsiflexion.

Plantar flexion

The contact line is located in the posterior third of the talar surface. The sagittal talar curvature radius now increases from lateral to medial, with a broad medial/median peak (Table 1). Similarly, the degree of congruity and width A(l_c) thus achieve high values in this medial/median region (Table 2, Fig. 6). While standing on the toes, the UAJ shows ideal contact behavior, as previously described by Reimann et al. [20]. The main foci of contact area and force transmission are now on the medial/median side.

These findings correspond with results of Calhoun et al. [1], Kura et al. [11], and Kimizuka et al. [9] in a qualitative manner.

Material and methods

We studied the extent of incongruity of the articular surface curvatures of the UAJ by performing sequential moldings with dimensional stability. Molding silicon and molding plaster are used routinely in dental practice. Their dimensional stability is well established [3]. The determination of sagittal net lines should comply with the joint's main functional direction. According to Inman [8] and Seiler [24], who expected the "axis of the upper ankle joint" to be perpendicular to the lateral rim of the talus, we set the first sagittal net line closely along this rim. This line was the source to construct analog cartographic nets on the talar *and* the tibial articulating surface. These "quasi-quadratic" meshes of both nets were equal. Based on the cartographic nets, the local curvatures of both surfaces could be related in positions of dorsal/plantar flexion.

Limitations of the study

The anatomic specimens under study had a high mean age. The expected [21] progressive flattening of the articular surfaces with age makes it probable that the observed sagittal incongruity may represent a lower limit for normal UAJ.

Clinical consequences

Our findings confirm the clinical experience to choose a medial approach just anterior to the malleolus medialis to inspect the tibiotalar articulating surfaces because the degree of congruity is minimal at that location (Table 2, Fig. 6).

The outcomes after treatment of high-energy pilon fractures are currently poor, and the optimal course of treatment is still controversial [15]. For example, it is controversial as to whether fixation of a fractured dorsal malleolus is necessary [5], [28]. Based on our results pertaining to the contact line in the UAJ, in the cases of pilon fractures or fractures of the posterior malleolus, the dorsal part of the tibial articular surface should be fixed indirectly or directly [5] because these parts are important in plantar flexion, for example, when climbing downstairs.

Because of the transversal congruity of the contact lines, eversion and inversion are only possible by dehiscence between tibia and talus. Because under full weight bearing, this dehiscence is reversed, inversion and eversion are blocked [26], thus stabilizing the joint. This mechanism is of interest not only for fracture treatment but also for designing total ankle prostheses. Prosthetic designs should account for the transversal linear contact of the upper ankle joint [13].

Discussion of the central questions of the study

1. The tibial net lines are invariably circular, but the corresponding talar net lines are non-circular. The corresponding shape depends on the medial/lateral and anterior/posterior contact positions.
2. The local sagittal curvature incongruity is primarily determined by the shape of the talar surface.
3. The transversal net lines are congruent. Hence, the incongruity of the articulating surfaces is given by the incongruity of the sagittal contours.
4. From dorsal to plantar flexion, the foci of contact area and force transfer are shifted from the lateral to the medial side.

5. Conclusions

Our morphological measurements show that a medial/lateral contact line normally exists between the tibial and talar articulating surface.

This contact line is responsible for a large contact area, which reduces the joint pressure and explains the joint's low rates of arthrosis [14], [16].

From dorsal to plantar flexion, the foci of contact area and force transfer are shifted from the lateral to the medial side.

In dorsiflexion, under the strained syndesmosis, the joint has only two sagittal degrees of freedom (dimeric chain [10], [17]).

In plantar flexion, the joint can resolve the linear contact by axial rotation. While standing on toes, rotation can be performed with small amplitudes.

In surgery, an exact anatomical reconstruction of the surfaces is necessary to preserve the contact line.

References

[1] CALHOUN J.H., LI F., LEDBETTER B.R., VIEGAS S.F., *A comprehensive study of pressure distribution in the ankle joint with inversion and eversion*, Foot Ankle Int., 1994, Vol. 15(3), 125–133.

[2] DUMONT C., ZIEHN C., KUBEIN-MEESENBURG D., FANGHANEL J., STURMER K.M., NAGERL H., *Quantified contours of curvature in female index, middle, ring, and small metacarpophalangeal joints*, J. Hand Surg. Am., 2009, Vol. 34(2), 317–325.

[3] EAMES W.B., WALLACE S.W., SUWAY N.B., ROGERS L.B., *Accuracy and dimensional stability of elastomeric impression materials*, J. Prosthet. Dent., 1979, Vol. 42(2), 159–162.

[4] FICK R.A., *Handbuch der Anatomie und Mechanik der Gelenke*, Fischer Verlag, Jena 1904, 405–444.

[5] FORBERGER J., SABANDAL P.V., DIETRICH M., GRALLA J., LATTMANN T., PLATZ A., *Posterolateral approach to the displaced posterior malleolus: functional outcome and local morbidity*, Foot Ankle Int., 2009, Vol. 30(4), 309–314.

[6] HANSEN C.C., *Zur Biomechanik des oberen Sprunggelenkes*, University of Göttingen, Göttingen 2001.

[7] HORISBERGER M., VALDERRABANO V., HINTERMANN B., *Posttraumatic ankle osteoarthritis after ankle-related fractures*, J. Orthop. Trauma, 2009, Vol. 23(1), 60–67.

[8] INMAN V., *The joints of the ankle*, Williams & Williams, Baltimore 1976.

[9] KIMIZUKA M., KUROSAWA H., FUKUBAYASHI T., *Load-bearing pattern of the ankle joint. Contact area and pressure distribution*, Arch. Orthop. Trauma Surg., 1980, Vol. 96(1), 45–49.

[10] KUBEIN-MEESENBURG D., NAGERL H., COTTA H., FANGHANEL J., *Biomechanical principles in diarthroses and synarthroses. I: Basic concepts in diarthroses*, Zeitschrift für Orthopädie und ihre Grenzgebiete, 1993, Vol. 131(2), 97–104.

[11] KURA H., KITAOKA H. B., LUO Z.P., AN K.N., *Measurement of surface contact area of the ankle joint*, Clin. Biomech. (Bristol, Avon), 1998, Vol. 13(4–5), 365–370.

[12] LANDAU L.D., LITSCHITZ E.M., *Elastizitätstheorie, Lehrbuch der theoretischen Physik*, H.G. Schöpf (ed.), Frankfurt 2010.

[13] LEARDINI A., CATANI F., GIANNINI S., O'CONNOR J.J., *Computer-assisted design of the sagittal shapes of a ligament-compatible total ankle replacement*, Med. Biol. Eng. Comput., 2001, Vol. 39(2), 168–175.

[14] MEDLEY J.B., DOWSON D., WRIGHT V., *Surface geometry of the human ankle joint*, Eng. Med., 1983, Vol. 12(1), 35–41.

[15] MICHELSON J.D., *Fractures about the ankle*, J. Bone Joint Surg. Am., 1995, Vol. 77(1), 142–152.

[16] MUEHLEMAN C., MARGULIS A., BAE W.C., MASUDA K., *Relationship between knee and ankle degeneration in a population of organ donors*, BMC Med., 2010, Vol. 8, 48.

[17] NAGERL H., KUBEIN-MEESENBURG D., COTTA H., FANGHANEL J., *Biomechanical principles of diarthroses and synarthroses*. III: *Mechanical aspects of the tibiofemoral joint and role of the cruciate ligaments*, Zeitschrift für Orthopädie und ihre Grenzgebiete, 1993, Vol. 131(5), 385–396.

[18] NAGERL H., WALTERS J., FROSCH K.H., DUMONT C., KUBEIN-MEESENBURG D., FANGHANEL J., WACHOWSKI M.M., *Knee motion analysis of the non-loaded and loaded knee: a re-look at rolling and sliding*, J. Physiol Pharmacol., 2009, Vol. 60 Suppl. 8, 69–72.

[19] PAAR O., RIECK B., BERNETT P., *Experimental studies on load-bearing pressure and contact areas in the ankle joint*, Unfallheilkunde, 1983, Vol. 86(12), 531–534.

[20] REIMANN R., ANDERHUBER F., GEROLD J., *The geometry of the human trochlea tali*, Acta Anat. (Basel), 1986, Vol. 127(4), 271–278.

[21] RIEDE U.N., MULLER M., MIHATSCH M.J., *Biometric studies elucidating the pathogenesis of arthrosis exemplified by the ankle joint*, (author's transl.), Arch. Orthop. Unfallchir, 1973, Vol. 77(3), 181–194.

[22] SCHAEFER K.L., SANGEORZAN B.J., FASSBIND M.J., LEDOUX W.R., *The comparative morphology of idiopathic ankle osteoarthritis*, J. Bone Joint Surg. Am., 2012, Vol. 94(24), e181.

[23] SCHMIDT H.M., *The articular surfaces of the human ankle joint*, Adv. Anat. Embryol. Cell. Biol., 1981, Vol. 66, 1–81.

[24] SEILER H., *Biomechanics of the upper ankle joint*, Orthopade, 1986, Vol. 15(6), 415–422.

[25] STAUFFER R.N., CHAO E.Y., BREWSTER R.C., *Force and motion analysis of the normal, diseased, and prosthetic ankle joint*, Clin. Orthop. Relat. Res., 1977, Vol. 127, 189–196.

[26] STORMONT D.M., MORREY B.F., AN K.N., CASS J.R., *Stability of the loaded ankle. Relation between articular restraint and primary and secondary static restraints*, Am. J. Sports Med., 1985, Vol. 13(5), 295–300.

[27] VALDERRABANO V., HORISBERGER M., RUSSELL I., DOUGALL H., HINTERMANN B., *Etiology of ankle osteoarthritis*, Clin. Orthop. Relat. Res., 2009, Vol. 467(7), 1800–1806.

[28] VAN DEN BEKEROM M.P., HAVERKAMP D., KLOEN P., *Biomechanical and clinical evaluation of posterior malleolar fractures. A systematic review of the literature*, J. Trauma, 2009, Vol. 66(1), 279–284.

[29] VELJKOVIC A., NORTON A., SALAT P., SALTZMAN C., FEMINO J., PHISITKUL P., AMENDOLA A., *Lateral talar station: a clinically reproducible measure of sagittal talar position*, Foot Ankle Int., 2013, Vol. 34(12), 1669–1676.

[30] WINDISCH G., ODEHNAL B., REIMANN R., ANDERHUBER F., STACHEL H., *Contact areas of the tibiotalar joint*, J. Orthop. Res., 2007, Vol. 25(11), 1481–1487.